Geophysical Survey at St Helena School, Sheepen Road, Colchester, Essex
DRAFT

NGR TL 8836 5850

August 2014

Dr T J Dennis
Byrches, Craxes Green, Birch, Colchester CO2 0NS
tim@essex.ac.uk

Abstract

A magnetometer survey was conducted in July/August 2014 over the major part of playing fields associated with St Helena School, where installation of an all-weather playing surface is planned. The western and southern parts of the field are known to be occupied by Roman and late Iron Age structures, including a large Roman temple within an extended precinct wall and a smaller Roman temple near the northwestern border. The results confirm the general pattern of occupation. Bordering Westway, the eastern part of the field in contrast shows a dense and unstructured scatter of anomalies probably caused by ferrous debris, the origin of which cannot be determined without excavation. Features of archaeological origin are present, especially at the western end. Not part of the formal assignment, but used as an evaluation opportunity for a new instrument, a ground penetrating radar survey over an area 80 by 40 m at the extreme west of the site shows additional structured features mostly distinct from those identified by the magnetometer.

Introduction

A magnetometer survey was carried out on behalf of Colchester Archaeological Trust (CAT) over St Helena School playing field. The principal target was the eastern section where new playing surfaces are planned, and identified in Fig. 1, but as much as possible of the field was also covered in a pattern of 30x30 m blocks. Fig. 2 shows the nominal target area as laid-out by CAT, including an overlay of known and conjectured archaeological features based on the work of Hawkes and Hull, and other sources including aerial photographs. The main reference works on previous archaeological investigations related to the site are listed below[1].

The work was carried out between 21 and 23 July 2014. The magnetometer is sensitive to changes of temperature, which can lead to spurious changes in signal level that have to be suppressed in post-processing. Mostly stable ambient temperatures during this survey coupled with high amplitude anomalies mean that little remedial processing has been required.

The ground penetrating radar sample survey was carried out in two sessions during August 2014 and covered the western part of the site, including part of the Roman temple precinct wall excavated in 1935.

1 *Camulodunum, First Report on the Excavations at Colchester, 1930-1939*. Hawkes, C. F. C. and Hull, M. R., Society of Antiquaries, XIV, London, 1947.

Roman Colchester. Hull, M. R., Society of Antiquaries, XX, London, 1958.

Methodology

The instrument used was a Geoscan Research type FM256. The FM256 is a gradiometer type, meaning that the output is the *difference* in the magnitude of the vertical component of the local Earth's magnetic field taken between fluxgate magnetic field sensors 0.5 m apart vertically. The output is in nanotesla, nT, and the instrument was operated on its most sensitive range where the minimum detectable difference is 0.05 nT (for comparison, the vertical component of the Earth's field at latitudes in the UK is in the region of 44000 nT[2]). For detailed information on sources of magnetic anomalies in the landscape, see for example Clark's *Seeing Beneath the Soil*[3]. In summary, soils with higher magnetic susceptibility than the local average generate positive anomalies, and vice versa. Soils that are rich in magnetotactic bacteria, such as occur in areas of human activity, generate positive anomalies, particularly where topsoil (or topsoil backfill) is thicker than normal such as within ditches or post holes. Other sources of anomalies, usually of high or overload amplitude, are ferrous debris of any kind.

The survey was conducted in the standard way recommended by Geoscan Research[4], which means a guide string with markers at 1 m intervals is set up between tape measures on the edges of each block, perpendicular to the traverse direction. The operator initiates the recording process then walks parallel to the string and 0.5 m from it at such a speed that its 1 second timing bleeps synchronise with the markers. The survey grid was laid out in an approximately east-west orientation. The zig-zag traverse method was used, the first track heading west from the southeast corner. Block size was 30 x 30 m.

Although the nominal block size was 30 x 30 m, in practice output quality is improved if two or more blocks can be surveyed and processed as one, so when possible the areas were covered in unbroken sections of 60 or 90 traverses of 30 m. In addition, coverage was sometimes extended beyond the limits of the survey grid, especially along its northern edge.

Fig. 3 shows the instrument in use on the site.

Fig. 4 is a plot of Total Station measurements on peripheral points of the survey grid as previously laid-out by CAT staff. For reference it also includes salient points on corners of buildings, the eastern fence of the tennis courts and the peripheral fence to the north and east of the site. The coordinate system is in metres with arbitrary origin, and is used for subsequent site plans.

Fig. 5 gives the layout, dimensions and sequencing of the survey blocks. Note that block 11 overlaps block 9 by 10 m. Where this occurs the software takes the average of replicated sample values which reduces 'noise' by 3 dB.

Parameters summary

Traverse length	30 m
Traverse spacing	1 m
Sample density in traverse direction	8 m^{-1}
Traverse speed	1 $m.s^{-1}$.
Instrument sensitivity	0.1 nT

2 Source: http://www.geomag.bgs.ac.uk/data_service/data/bulletins/bulletins.html

3 *Seeing Beneath the Soil prospecting methods in archaeology*, A. Clark, Routledge, London, 2000. ISBN 0-415-21440-8 or later editions.

4 FM256 Instruction Manual Version 1.6, Geoscan Research, May 2004

Signal Processing

The raw data samples are stored in the magnetometer, and subsequently downloaded. Data from each day's work are saved in a single file in the order of capture, irrespective of the associated block structure. (The raw data format as saved is given in the Appendix). To access an individual block, an offset into the data sequence is specified, then the appropriate number of active samples read-in. Software is Unix-based, and supports a range of geophysical survey data types with signal processing methods developed by the author since the early 2000s from experience with practical survey datasets.

Processing uses some or all of the following stages.

1. Extract data for individual survey block from the instrument dump file. Clip extreme values as necessary. Sample points that exceed the clipping limits (+ve and -ve) are ignored in subsequent processing, and in the output image set to 'transparent'. Rectangular regions of a block can also be deleted in this way.

2. Alternate track reversal. Essential to correct for the zig-zag scanning format of the survey. Assuming tracks are numbered from zero, tracks 1, 3... are reversed.

3. 'Destagger'. Usually required to correct for systematic operator- and direction-dependent longitudinal positional offsets.

4. A form of mean level subtraction. Essential. The instrument outputs the difference in signal amplitude from its two fluxgate sensors; after initial alignment[5] and 'Set Zero', this should be zero, but there is typically a drift with time, usually a result of change in ambient air temperature, or differential heating, and hence distortion, of the instrument casing from exposure to sunlight.

A range of options is available:

   i. Overall mean level subtraction. The minimum necessary. Guarantees the mean level of each data block will be zero, but unwanted variations within a block remain.

   ii. Direction-dependent mean level subtraction. Odd and even track set averages computed and subtracted independently. This largely removes direction- and operator-dependent signal offsets.

   iii. Direction-dependent smoothed track average mean level subtraction. Individual track averages are calculated, then the sets of values for odd and even tracks separately smoothed with a Gaussian lowpass filter, the 'standard deviation' of which specifies the width of the smoothing window. Values up to 2 are typical. A value of zero does no smoothing, so defaults to individual track average subtraction. This removes nearly all track-dependent variation, but also suppresses any 'real' feature that happens to be parallel to and longer than a track. A value of 1 is the typical compromise choice.

5. **Post filtering**. Optional, but useful in situations where 'genuine' anomalies have very low amplitude, which is common on gravel soils. The final output image for a block is generated from a weighted average of heavily smoothed and original pictures. The smoothing is done with circular-footprint Gaussian filters, where the 'standard deviation' measure is equivalent to 1 to 2 m. on the ground. Very approximately, the diameter of the smoothing window is hence 2-4 m.

5 Full procedure in FM256 manual, *ibid*.

Output = A.original + B.smoothed

In normal usage, A + B = 1; for smoothing applications, typical values are A = 0.3, B = 0.7. These values mean that the video dynamic range for 'large' features (> 2-4 m in extent) is unaffected, but for small ones (<≈1 m) has amplitude multiplied by 0.3.

6. **Output video level**. Essential. A processed block is output as an uncompressed greyscale image, where video levels are represented in 8 bit with black represented as 0 and white 255. Internally, the signals are represented and processed in signed double precision floating point. To convert to standard 8-bit greyscale video, the desired overall range is specified, e.g. 10 nT. This would be interpreted as -5 nT to +5 nT, with hard-limiting of values outside this range. This is then scaled to -128.0 to +127.0, and an offset of +128.0 added, which gives the normal video range in which magnetometer zero level is represented on the picture as mid grey. The processed sample values are converted to 8-bit unsigned integers for video. Specifying -10 nT range reverses the output contrast to what is usual for magnetometer imagery where positive anomalies (usually the ones of interest) are typically black, negative white.

7. **Mosaic layout**. Essential. Individual 'tiles' of the survey are assembled on a background which can contain a graticule, labelled axes, captions and other images. The tiled area can be lowpass filtered as well, which helps conceal block boundaries. Postfilter was not needed here.

Magnetometry results

A notable feature of this survey compared with others in the surrounding rural areas is the high amplitude of anomalies that are likely to be of archaeological origin. It also has a general level of spurious anomalies characteristic of urban areas. These appear as bipolar (black/white) spot features, due to small ferrous objects in the topsoil which act as randomly oriented magnets; fired clay can have a small permanent magnetic field so tile or brick fragments are an additional potential source. An extended 'glow' from large iron-containing structures nearby can also occur, for example from fences or buildings. In this survey, the rectangular windowing-out feature has been used to reduce their impact, especially along the southern edge near the school itself.

Fig. 6 shows the results with minimal processing and black to white video range corresponding to +50 to -50 nT respectively.

Fig. 7 is similar (details in figure caption) but with the dynamic range reduced to ±15 nT to increase contrast.

The magnetometer survey area divides into distinct regions, close to the northeastern boundary and everywhere else. The first contains unstructured and dense clusters of spot ferrous anomalies, and has a distinct boundary running southeast to northwest to the rest of the site. The transition is marked by a lower-level broad linear positive anomaly: 19th century maps show the site to have been agricultural land[6], and the feature is likely to match a field boundary of that time. Indeed, it is probably visible in the illustration shown in Fig. 8 as a line of trees in the near background; given that the site is low-lying and on the flood plain of the Colne, it is likely there was also a drainage ditch, now backfilled.

Pairs of overload level anomalies in various places on the field correspond to steel tubes set into the soil and used as permanent sockets for goal posts. A prominent 'D' shaped positive (but not overload-level) anomaly is visible on the surface as a change in appearance of the grass. Beneath the surface is coarse grit and the feature is thought to be a former base for such as discus or hammer throwing.

The western section of the site is densely covered by structured anomalies, mostly positive, that are archaeologically significant. Figs. 9a and 9b allow comparison between the magnetometry image and the detailed plan of the 1935 excavations reported by Hull[7]. A negative anomaly (white line) corresponds to the large temple precinct wall, constructed from stone and fully excavated by Hull – the excavated remains of the temple are in the foreground of Fig. 8. Such anomalies are unusual, and occur when the associated feature is *less* magnetic than its surroundings. Stone has this property.

A linear feature parallels the northwestern aspect of the precinct, and corresponds to a known Roman road; a similar feature, at first parallel to the road, diverges from it and appears to curve west immediately south of the small temple at the edge of the site. The magnetometry does appear to pick-up parts of its concentric foundations.

6 See for example Ordnance Survey 6 inch series, Essex Sheet XXV11, 1881. A high-quality scan can be downloaded from http://maps.nls.uk/view/102341873 but is not reproduced here for copyright reasons.
7 Hull, M. R. 1958. *ibid*.

Ground Penetrating Radar trial

Principle of GPR. The system we used is an Utsi Groundvue 3. The white box in contact with the ground (Fig. 10, showing it in operation, being towed by a modified mobility scooter.) contains downward-pointing transmit and receive antennas. GPR works on exactly the same principle as a conventional navigational radar: the transmitter generates a series of very brief radio frequency single pulses while the receiver 'listens' for echoes. The difference from conventional radar is that the time delays before the echoes return are relatively small – tens of nanoseconds – so the signal waveform that represents the reflection profile has to be built-up from many individual pulses. Just as happens when light is partially reflected from a sheet of glass, any discontinuity – like a buried wall foundation – will reflect RF energy. Penetration of radio waves into soil is very poor, especially when wet, so longer-delayed echoes can be weak.

The sequence of profile waveforms is encoded digitally and sent via a wifi link to a laptop computer carried by the scooter – this technique has an advantage in that it isolates the GPR from potential electrical interference. The timing of profile capture is under control of a shaft encoder attached to the sense wheel at the rear of the radar box.

For the GPR trial, two blocks, nominally 40x40 m, on the western section of the St Helena School site were surveyed on 1 and 8 August 2014.

Survey parameters

Antenna centre frequency	400 MHz
Time window	40 ns.
Time samples per profile	256
Track spacing	0.5 m
Track length	40 m
Sample spacing along-track	25 mm (i.e. 40 samples/m)

Signal processing. Each track generates data that can be interpreted as a two-dimensional vertical slice with the horizontal axis representing distance and the vertical axis round-trip reflection time, increasing downwards to a maximum of 40 ns. Knowing the propagation velocity of radio frequency energy in the soil gives an estimate of depth. Velocity is given by $V = c.\sqrt{E_r}$ where c is the velocity of light in free space and E_r is the relative dielectric constant of the soil.

E_r depends on soil type and water content, both of which typically vary with depth, so the resulting depth values obtained from the time data are always extremely approximate. However, a good estimate of E_r for sandy moderately dry soils (as on this site) is 10 which with $c = 0.3$ m. ns^{-1} makes $V \approx 0.1$ m.ns^{-1}. Because the radar measures the round trip delay, 40 ns is hence equivalent to a maximum depth of 2 m.

On completion of the survey, the vertical slices and comprise a 'volume' like a pack of cards on edge, with X and Y spatial axes parallel to the ground surface and a time, T, or Z axis representing depth. We then take a series of horizontal slices, 'timeslices', which give a plan of sub-surface features; these are best viewed as an animated sequence when inter-layer relationships also become clear. Processing involves some filtering in the X, Y and T directions, but mainly has to account for the wide dynamic range of the raw received signals: near-surface reflections are very large but their amplitude falls rapidly with depth. For the examples reproduced here, which show the amplitude of the signals, the average signal over each timeslice is measured, then a varying gain correction applied to maintain a constant signal level over all slices. This inevitably results in increasing noise for the lower slices but enables useful results to be displayed within the limited video range available.

Results. Figs. 11 and 12 show example timeslice images. Black indicates the strongest reflections which would normally be caused by a relatively uniform and dense buried surface layer. The slight contrast in 'quality' of the two survey blocks, which were done on different days, is probably caused by a change in soil moisture level. Fig. 11 comes from a depth of about 0.7 m, Fig. 12 from 1.6 m. The most obvious feature is the very strong signal from the temple precinct wall, which has sufficient detail to show the alternating buttresses. Immediately northwest of the temple enclosure is an area of low-contrast 'background' where the main structures are indicated by an *absence* of signal. If this image is compared with the magnetometer result of Fig. 7 and also shown on Fig. 13, the GPR voids tend to correspond to strong features on the magnetometry. A possibility is that these features are shallow channels backfilled with a uniform organic-rich matter which would give good magnetic response but little or nothing on GPR. Away from the channels there is a moderate GPR response from the natural gravelly undersoil.

Particularly significant may be a symmetrical 'winged' structure towards the northwest boundary, highlighted on the second picture – on the right wing there is hexagonal feature, which may also be present on the left. The central part of the survey area is dominated by a very high-contrast large-area feature, suggesting a patch of solid paving.

Fig. 12 is a timeslice from a substantially greater depth. The main interest here is what appears to be the layout of an unknown building, highlighted on the second image, together with an arc to its northwest - the arc is more clearly visible on slightly shallower timeslices. Both features appear to be on a different alignment to others on the site.

Conclusions

Both survey media have provided significant results, often of a complementary nature in that features on one are not always replicated in an obvious way on the other.

The 1935 excavators' work on other than the immediate vicinity of the temples was confined to a small number of long trenches (Fig. 9a) within and without the large temple precinct. A number of features were noted, and a general conclusion made that the area bordering the southwestern aspect of the wall had been the site of metal working. The magnetometry did not cover this section, but the area it did reach is densely occupied by structured anomalies that deserve further archaeological interpretation and evaluation.

The principal advantage of ground penetrating radar is its ability to reveal structures at greater depth than magnetometry, and more importantly their relative position with respect to the surface. This was demonstrated by strong indications of a building, possibly unrelated to and predating the known temple and its surroundings. In the absence of archaeological excavation, further GPR surveys should be carried out if possible.

Acknowledgements

Thanks to St Helena School for site access, Colchester Archaeological Trust for the initial site layout. Pauline Skippins shared the magentometer survey. Ben Crone, Louise Harrison, Les Peck, Aldous Rees and Adam Willis assisted with the GPR.

Appendix

FM256 data dumps. The raw data files that accompany this report are as follows (from a Unix directory listing):

Size (bytes)	Date of download	Name
324360	21 Jul 16:33	shs_210714.dat
499919	22 Jul 16:40	shs_220714.dat
127625	23 Jul 14:39	shs_230714.dat

Raw format (example as output by the instrument):

```
276
0
281
0
219
0
132
0
49
0
-10
0
-66
0
-134
0
-143
0
-120
0
.
.
.
```

Each sample is represented as a signed decimal number followed by a range code. The manufacturer specifies that if range is R, where $0 \leq R \leq 2$, data D, then the actual sample value, V, in nanotesla is computed from:

$V = D \cdot 0.5 \cdot 10^{R-1}$.

The first data value/range pair 276/0 hence represent 13.8 nT.

For valid data, $-4000 \leq D \leq +4000$. For range 0, the maximum signal range that can be recorded without overload is ±200 nT. In addition, the instrument represents unsampled data points (for example an uncompleted survey block or dummy points/tracks inserted manually) with D = +4095. The post-processing software takes this into account and can render such samples 'transparent' depending on the output image format.

Figure 1. Contractor's site plan

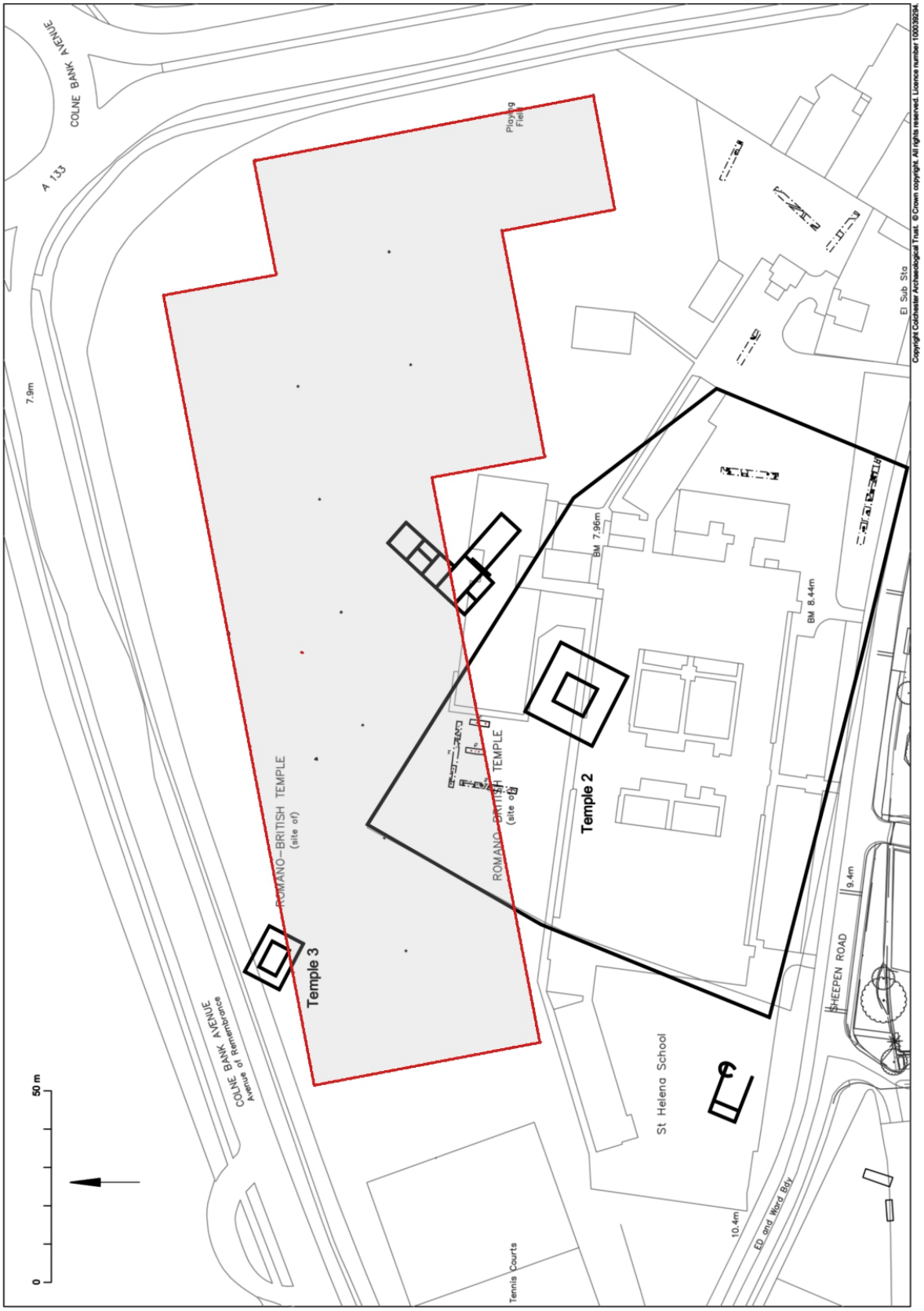

Figure 2. Magnetic survey nominal target area (grey) in relation to the site and archaeology. (CAT).

Figure 3. FM256 magnetometer in use. Marked guide string to operator's right.

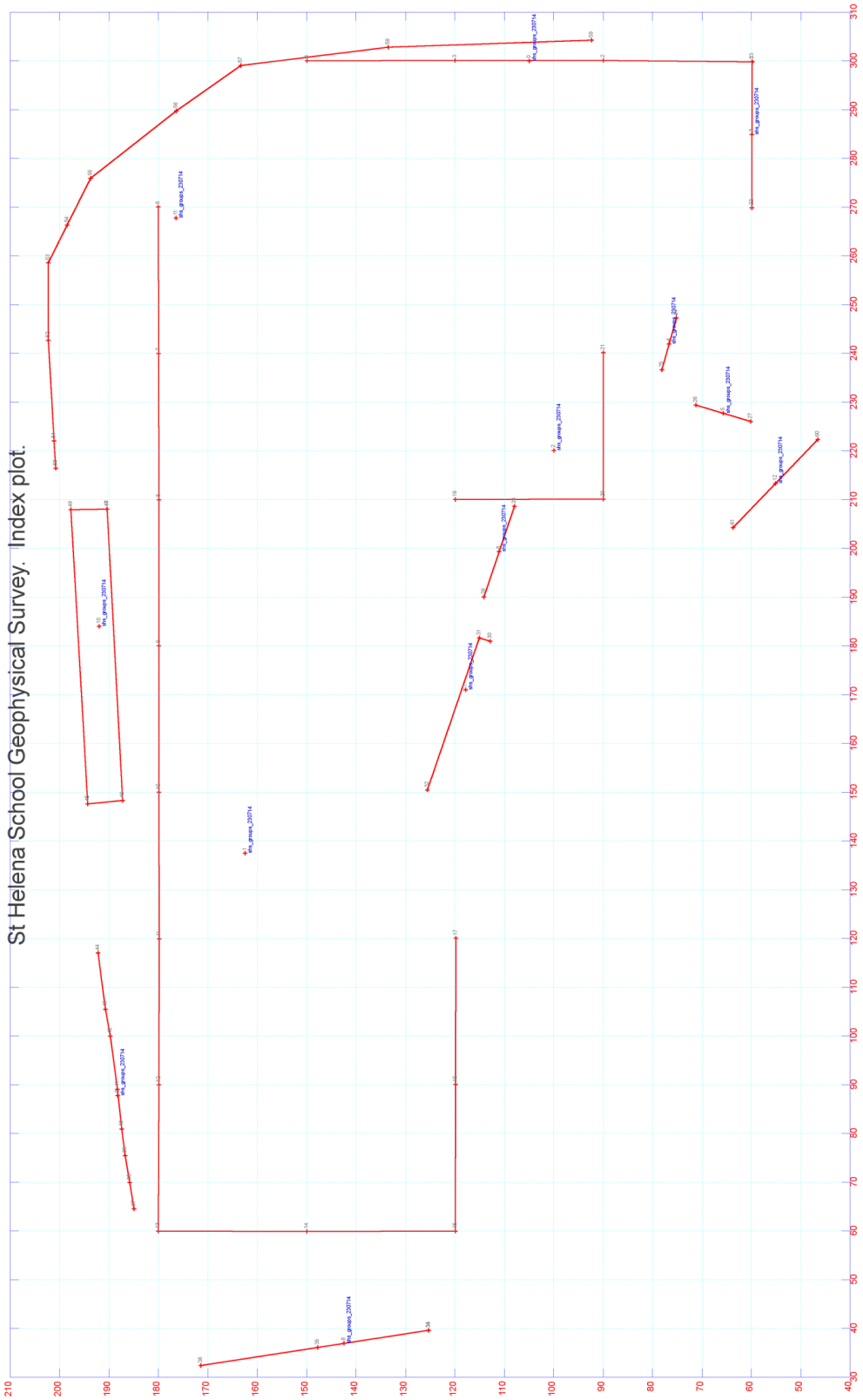

Figure 4. Total Station measurements, points labelled with measurement sequence number. 1-23 are the periphery of the survey grid as set-out by Colchester Archaeological Trust staff; 23 (SE corner) repeats 1 as a check.

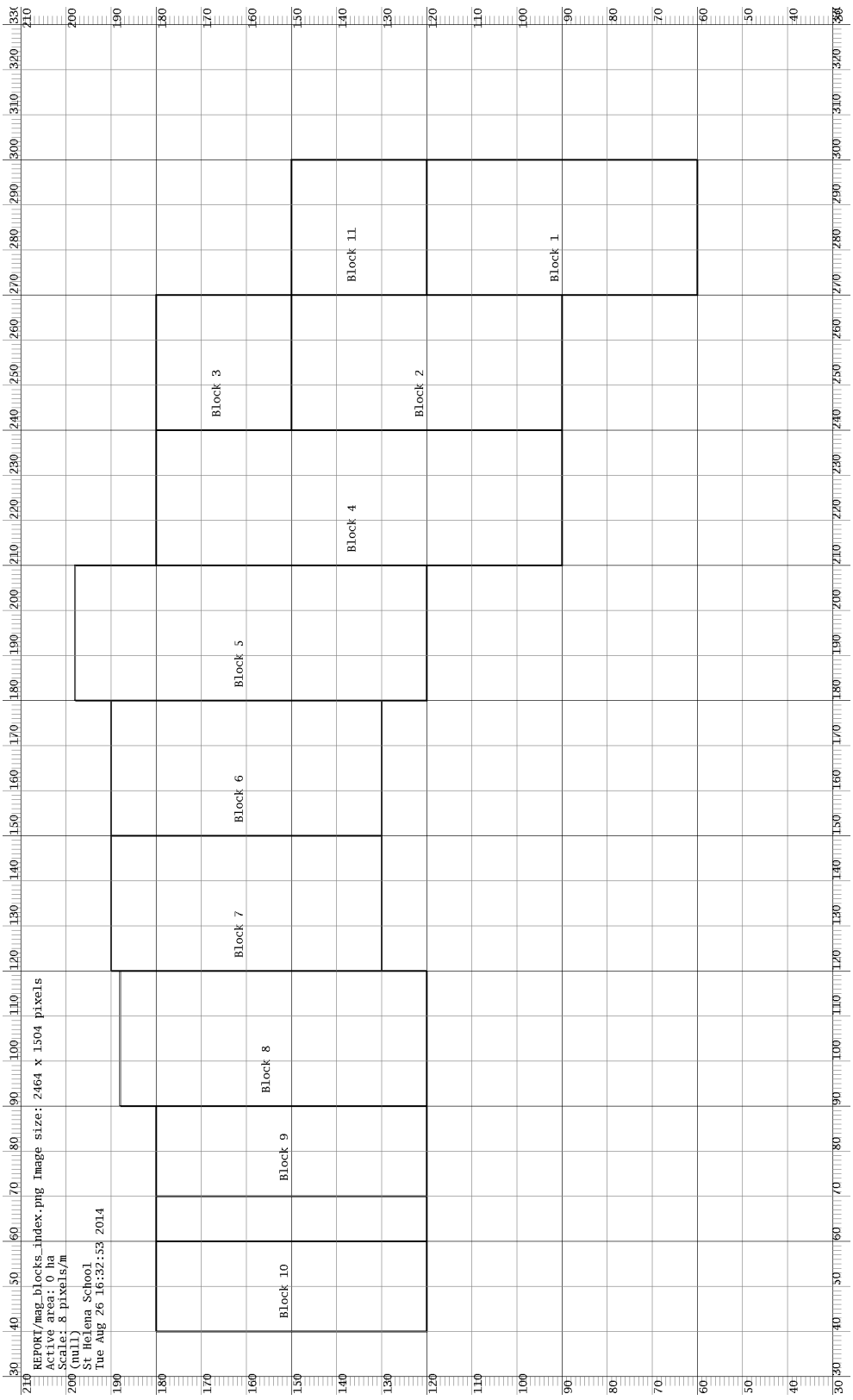

Figure 5. Magnetometer survey blocks layout and sequence.

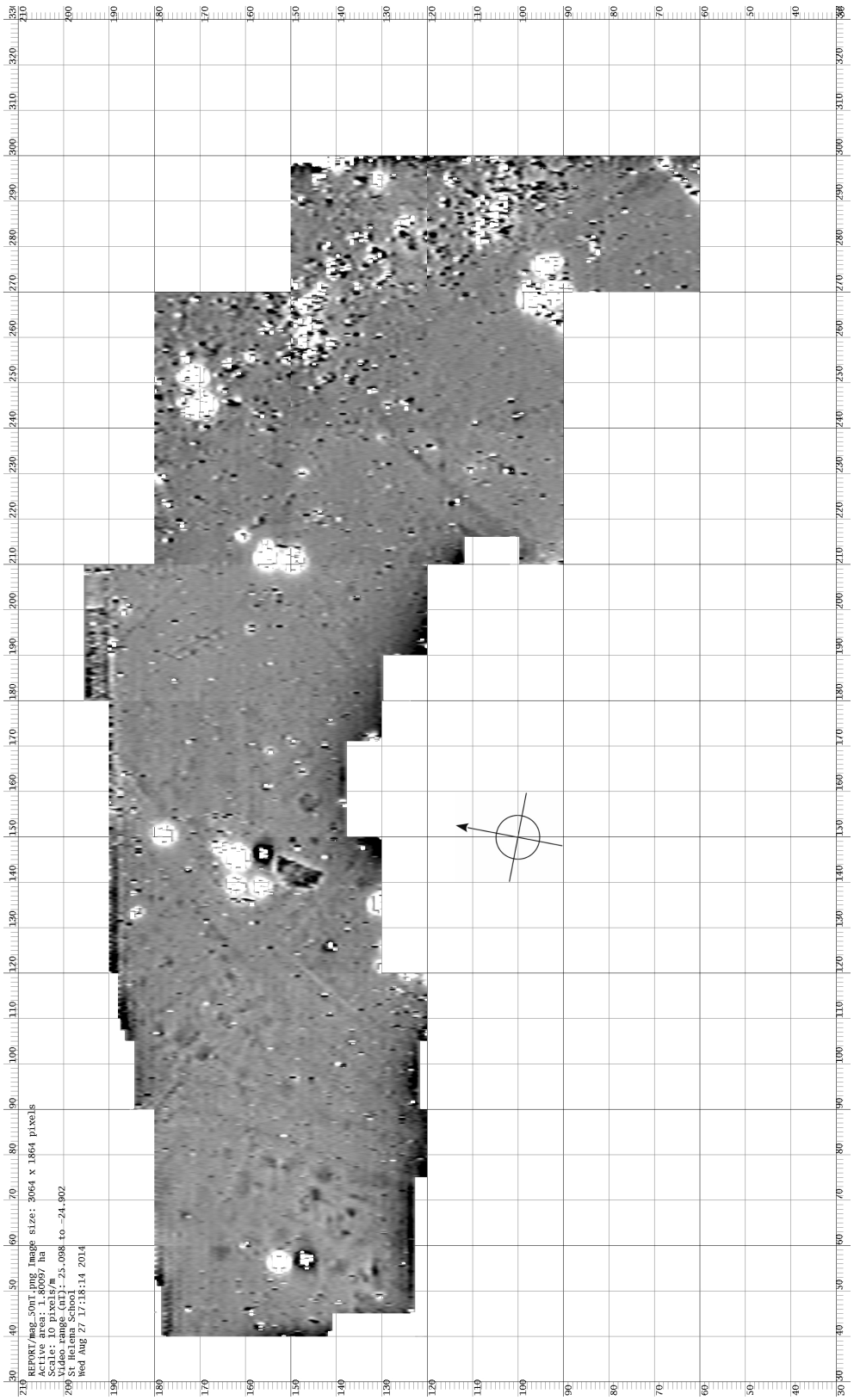

Figure 6. Destagger and block mean level subtraction only, dynamic range ±25 nT. Raw data clipping levels ±50 nT.

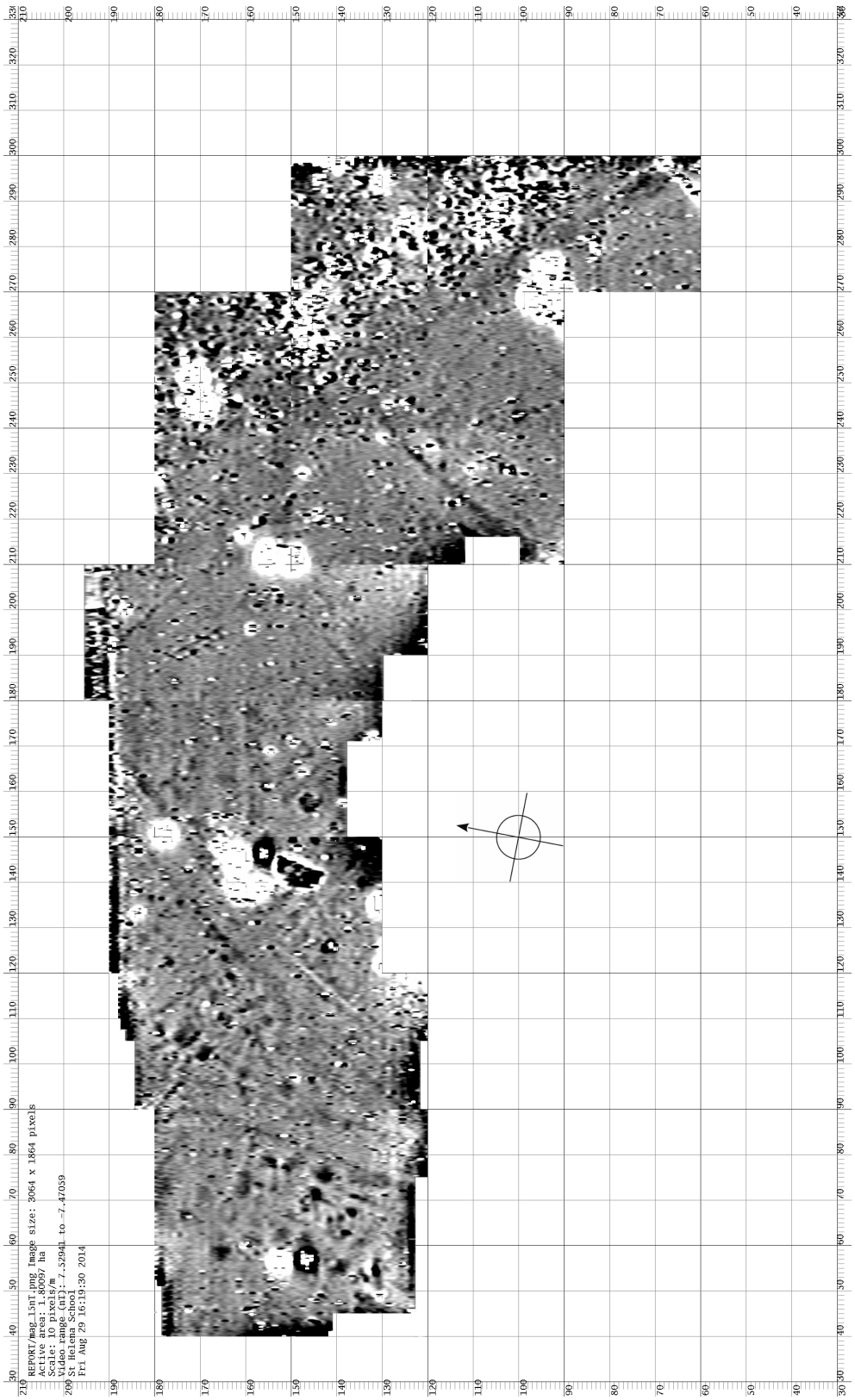

Figure 7. Based on Fig. 6, with addition of Gaussian-weighted local track mean subtraction. Dynamic range ±15 nT.

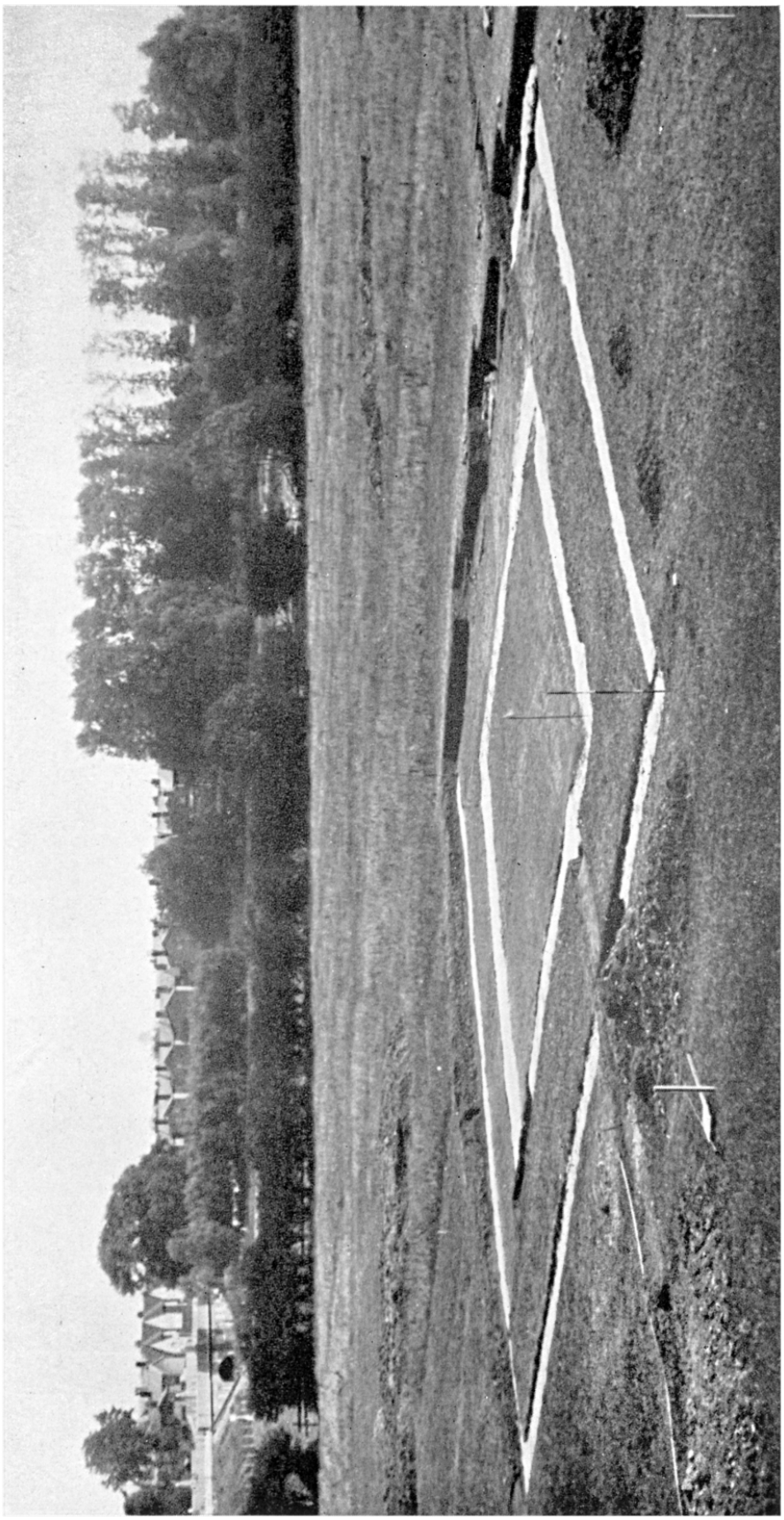

B. Site of the large temple from the SW. [95], pp. 224 ff.

Figure 8. Roman Temple excavation of 1935. A hedge marks a field boundary in the near distance. (Hull, M. R. 1958. *ibid*.)

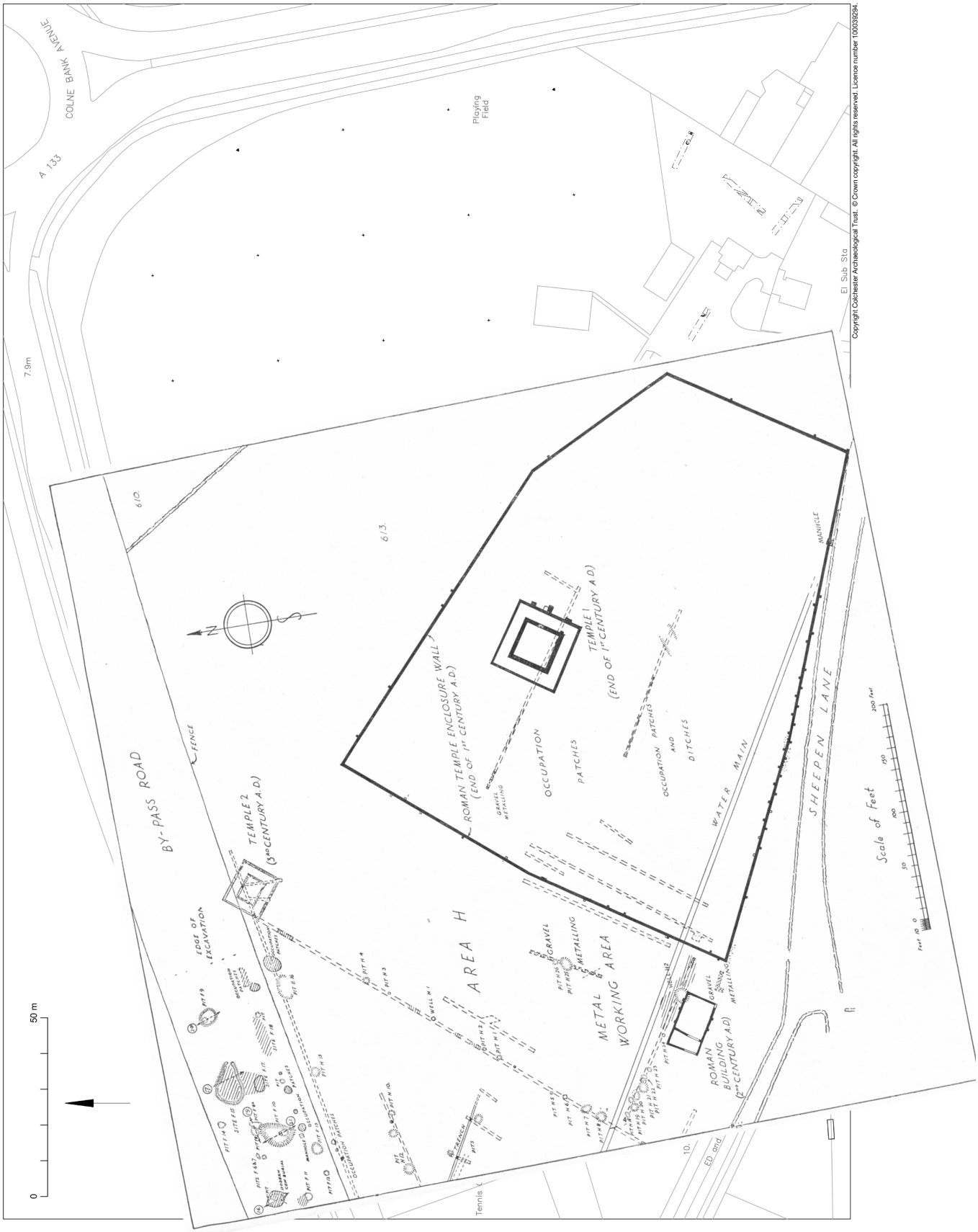

Figure 9a. Plan of Fig. 2 with aligned overlay of the 1935 excavation results. (Hull, M. R. 1958. *ibid*.)

Figure 9b. Fig. 9a with overlay of magnetometer survey result, dynamic range ±nT.

Figure 10. Ground penetrating radar system in use.

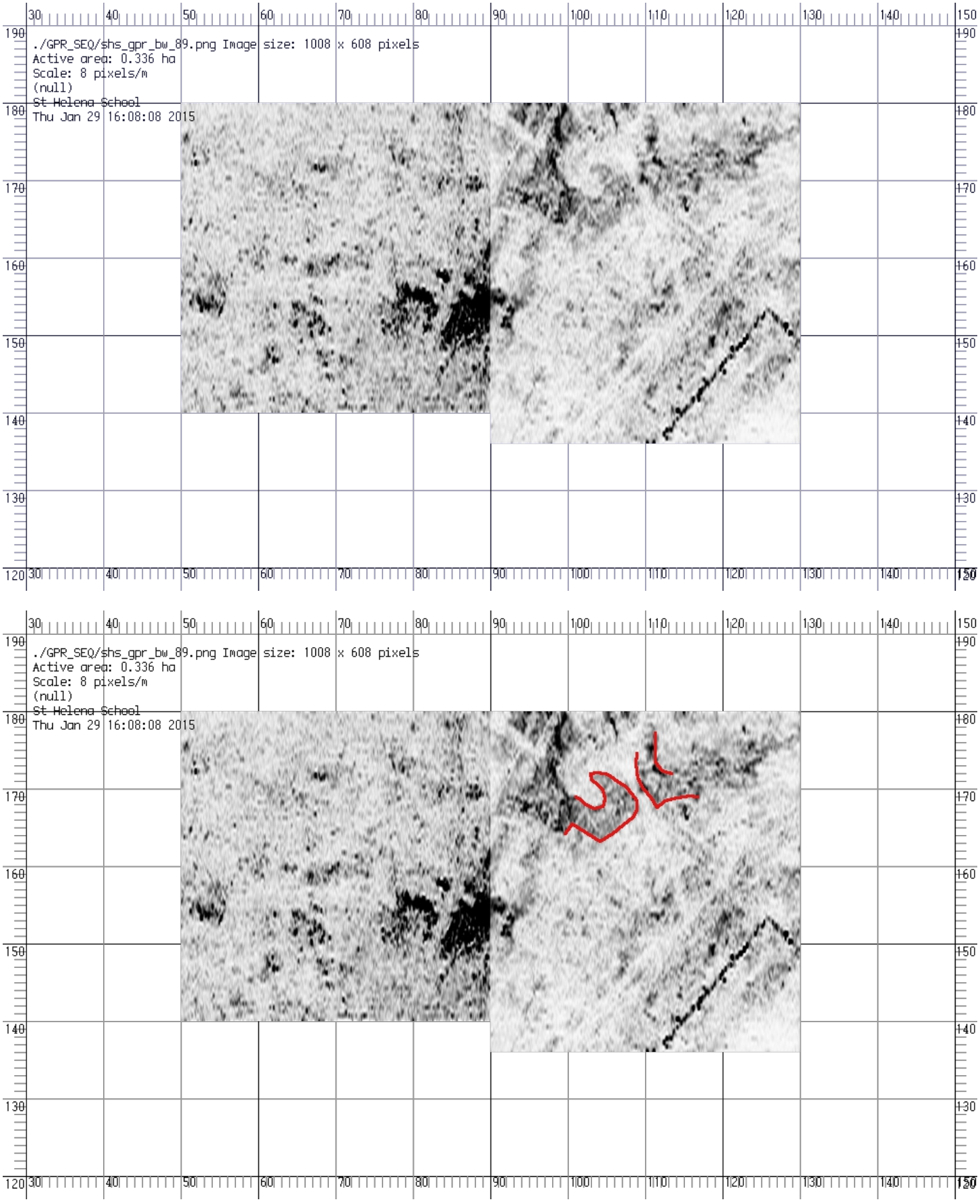

Figure 11. GPR timeslice image 89. Depth approximately 0.7 m

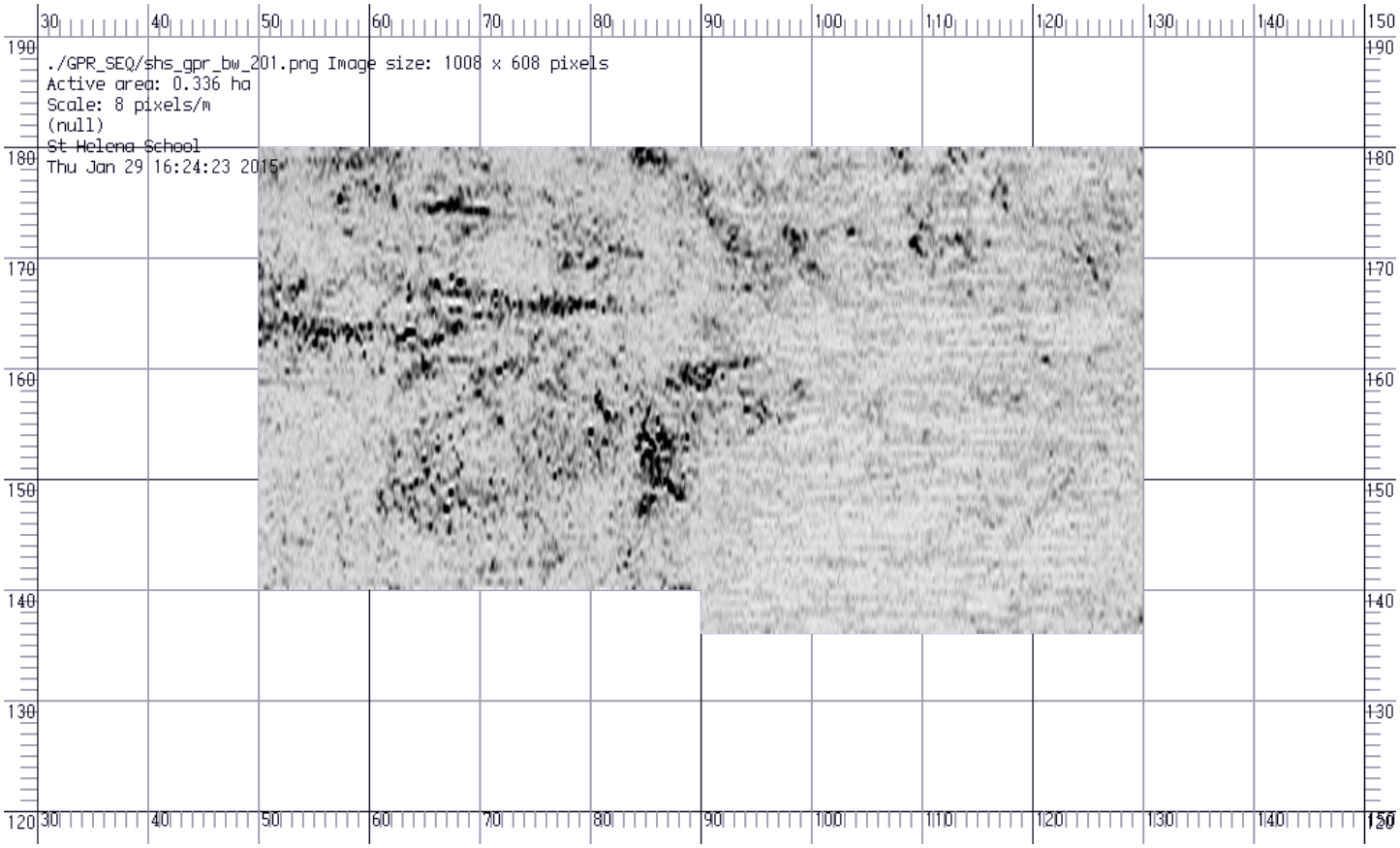

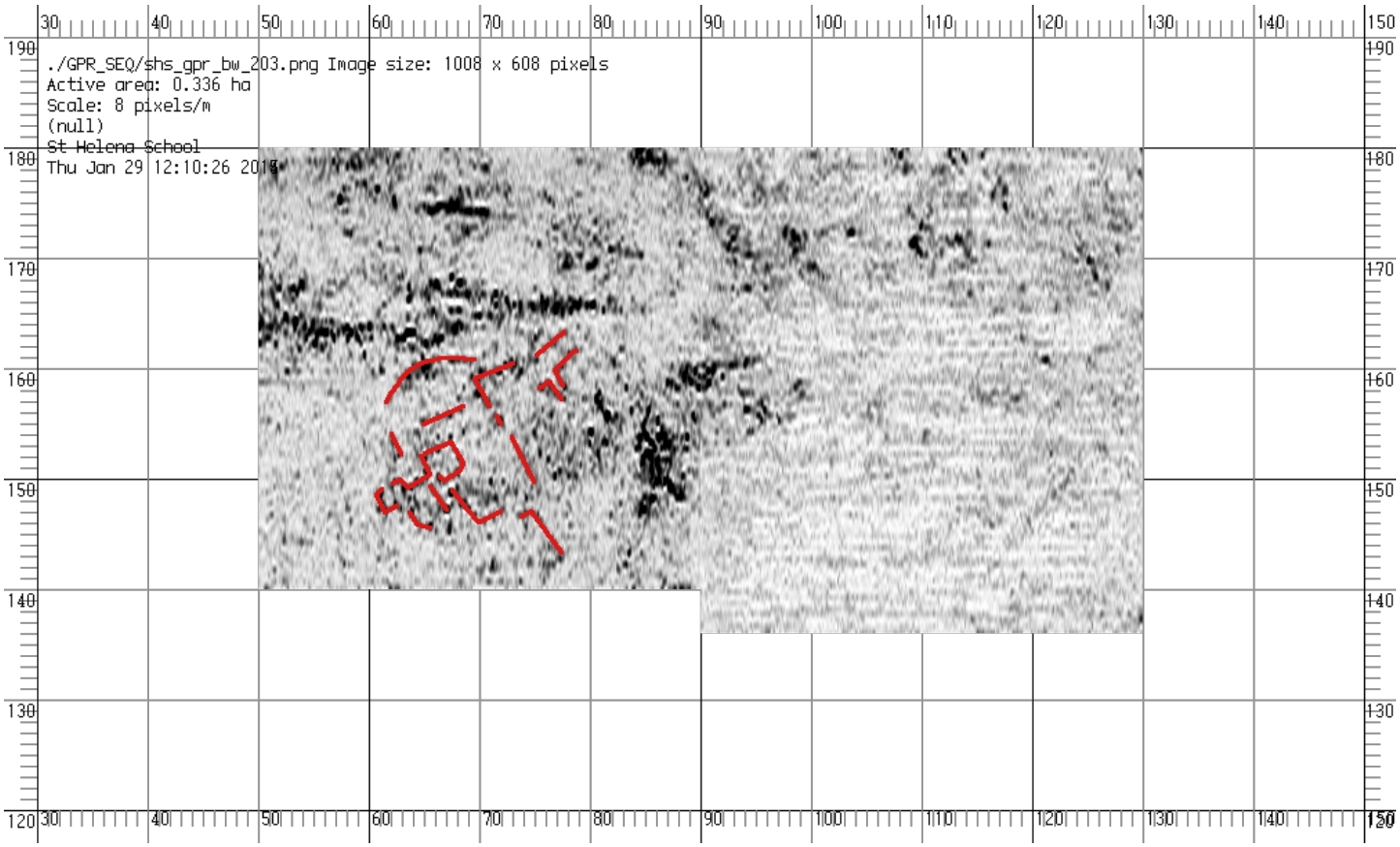

Figure 12. GPR timeslice image 201. Depth approximately 1.6m.

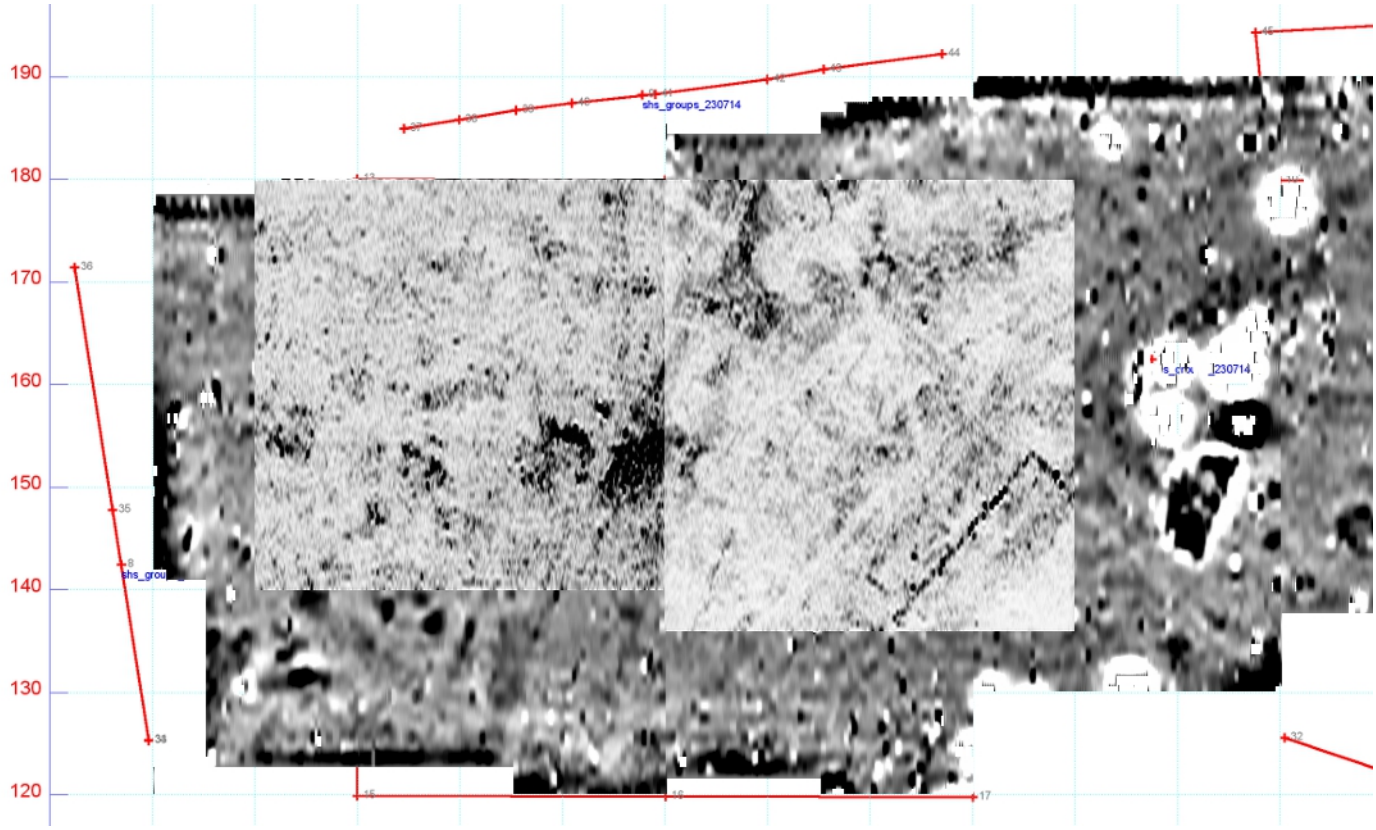

Figure 13a. GPR timeslice 95 overlayed on magnetometer image.

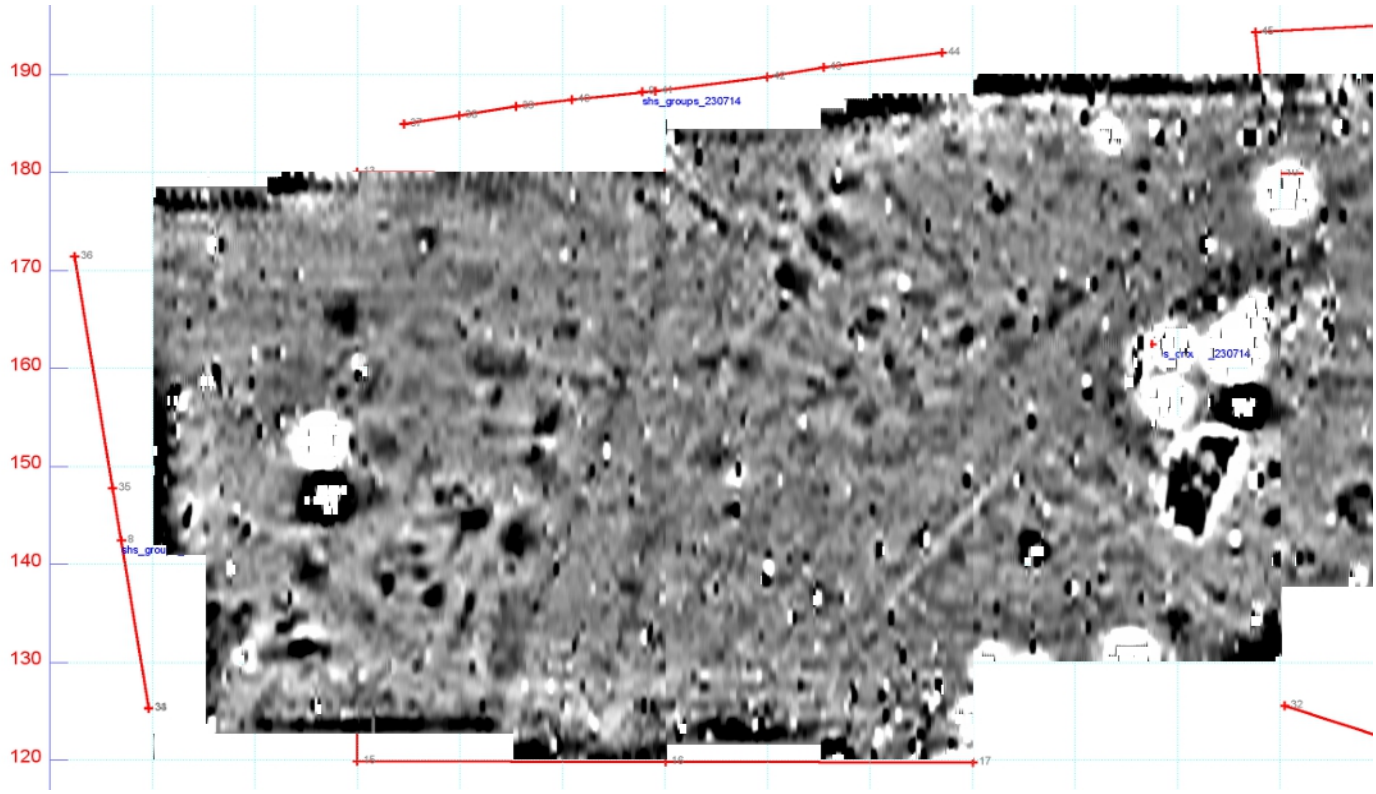

Figure 13b. Magnetometer image for comparison.